Earth's Future

RESEARCH ARTICLE
10.1029/2020EF001595

Changes in West African Summer Monsoon Precipitation Under Stratospheric Aerosol Geoengineering

C. Y. Da-Allada[1,2,3], E. Baloïtcha[2], E. A. Alamou[1], F. M. Awo[2], F. Bonou[2], Y. Pomalegni[2], E. I. Biao[1], E. Obada[1], J. E. Zandagba[1], S. Tilmes[4], and P. J. Irvine[5]

[1]LaGEA/ENSTP/UNSTIM, Abomey, Benin, [2]ICMPA-UNESCO Chair/UAC, Cotonou, Bénin, [3]LHMC/IRHOB, Cotonou, Bénin, [4]Atmospheric Chemistry, Observations, and Modeling Laboratory, National Center for Atmospheric Research, Boulder, CO, USA, [5]John A. Paulson School of Engineering and Applied Sciences, Harvard University, Cambridge, MA, USA

Abstract Stratospheric aerosol geoengineering (SAG) is suggested as a potential way to reduce the climate impacts of global warming. Using simulations from the Geoengineering Large Ensemble project that employed stratospheric sulfate aerosols injection to keep global mean surface temperature and also the interhemispheric and equator-to-pole temperature gradients at their 2020 values (present-day climate) under Representative Concentration Pathway 8.5 scenario, we investigate the potential impact of SAG on the West African Summer Monsoon (WASM) precipitation and the involved physical processes. Results indicate that under Representative Concentration Pathway 8.5, during the monsoon period, precipitation increases by 44.76%, 19.74%, and 5.14% compared to the present-day climate in the Northern Sahel, Southern Sahel, and Western Africa region, respectively. Under SAG, relative to the present-day climate, the WASM rainfall is practically unchanged in the Northern Sahel region but in Southern Sahel and Western Africa regions, rainfall is reduced by 4.06% (0.19 ± 0.22 mm) and 10.87% (0.72 ± 0.27 mm), respectively. This suggests that SAG deployed to offset all warming would be effective at offsetting the effects of climate change on rainfall in the Sahel regions but that it would be overeffective in Western Africa, turning a modest positive trend into a negative trend twice as large. By applying the decomposition method, we quantified the relative contribution of different physical mechanisms responsible for precipitation changes under SAG. Results reveal that changes in the WASM precipitation are mainly driven by the reduction of the low-level land-sea thermal contrast that leads to weakened monsoon circulation and a northward shift of the monsoon precipitation.

Plain Language Summary Stratospheric aerosol geoengineering is one of methods that could artificially reduce the amount of sunlight that reaches the Earth's surface in order to cool the planet. This method is identified as a possible means to reduce the climate impacts of global warming. One of the key variables affected by climate change is precipitation which is of great importance in monsoon regions such as West Africa. Here the potential impact of the stratospheric aerosol geoengineering on the West African Summer Monsoon precipitation and the associated mechanisms are investigated, using climate model simulations from the Geoengineering Large Ensemble project that used stratospheric sulfate aerosols injection to stabilize global mean surface temperature and, also, the interhemispheric and equator-to-pole temperature gradients at their 2020 values under RCP8.5 scenario. Results reveal that using stratospheric aerosol geoengineering, summer monsoon precipitation is nearly unchanged in the northern and southern Sahel regions compared to present day, whereas significantly decrease in monsoonal precipitation is noted in the Western Africa region. The relative contribution of the different mechanisms controlling changes in precipitation under stratospheric aerosol geoengineering is examined using the method of decomposition and results show that changes in precipitation are largely related to changes in the dynamic processes (monsoon circulation).

Key Points:
- We explore the potential impact of stratospheric aerosol geoengineering on the West African Summer Monsoon precipitation and the associated driving mechanisms
- Use of stratospheric aerosol geoengineering is effective for rainfall in the northern and southern Sahel whereas it is overeffective in Western Africa region
- Under stratospheric aerosol geoengineering, changes in the monsoon precipitation are mainly caused by changes in the dynamic processes (monsoon circulation)

Supporting Information:
- Supporting Information S1
- Figure S1

Correspondence to:
C. Y. Da-Allada,
daallada@yahoo.fr

Citation:
Da-Allada, C. Y., Baloïtcha, E., Alamou, E. A., Awo, F. M., Bonou, F., Pomalegni, Y., et al. (2020). Changes in west African summer monsoon precipitation under stratospheric aerosol geoengineering. *Earth's Future*, *8*, e2020EF001595. https://doi.org/10.1029/2020EF001595

Received 20 APR 2020
Accepted 1 JUN 2020
Accepted article online 11 JUN 2020

©2020. The Authors. Earth's Future published by Wiley Periodicals LLC on behalf of American Geophysical Union This is an open access article under the terms of the Creative Commons Attribution License, which permits use, distribution and reproduction in any medium, provided the original work is properly cited.

1. Introduction

West African summer monsoon (WASM) precipitation plays a key role in agriculture productivity, water supply, and energy generation and, therefore, is important to national economies of the region (Adarsh & Reddy, 2015; Odoulami & Akinsanola, 2017). WASM precipitation, which ranges from June to September/October on average (Akinsanola & Zhou, 2018; Haywood et al., 2013; Odoulami

& Akinsanola, 2017), is responsible for most precipitation over West Africa. Projections of future changes to the WASM suggest less rainfall over the western Sahel region and more rainfall over the central-eastern Sahel with the deficits driven by increasing air subsidence and the surplus by a more intense monsoon circulation (e.g., Akinsanola & Zhou, 2018; Monerie et al., 2012). Recently, studies of future projections also indicate a decrease of rainfall in the Sahel and increase of rainfall in the western Africa during the boreal summer (e.g., Soares et al., 2019). These projected changes in the WASM precipitation due to climate change could lead to major societal impacts such as increased vulnerability of water resources, health, catastrophic crop failures, and famine, among others (Akinsanola & Zhou, 2018; Giannini et al., 2018; Monerie et al., 2012; Soares et al., 2019).

Solar geoengineering (also known as solar radiation management), a set of proposals to artificially reduce the amount of solar radiation reaching the surface of the Earth, has been suggested as complementary approach to reducing the risks of global warming alongside more conventional approaches (e.g., Crutzen, 2006; Irvine et al., 2019; Jiang et al., 2019; Jones et al., 2018; Keith, 2000; Kravitz et al., 2017). It is shown that the use of stratospheric aerosol geoengineering (SAG), which consists of sulfur injection into the stratosphere, offers a unique potential to rapidly lower global temperatures (e.g., Crutzen, 2006; Jones et al., 2018; MacMartin et al., 2018; Tilmes et al., 2018). However, in most studies where SAG is deployed to offset all warming with regard to a certain baseline, it would more-than-offset the intensification of the hydrological cycle projected under global warming, which might increase climate risks for some regions (Bala et al., 2008; Irvine et al., 2019; Robock et al., 2008; Tilmes et al., 2013).

Most studies of SAG impacts on rainfall, using climate model simulations, have concluded that, if SAG is designed to offset all warming, global mean precipitation caused by global warming is reduced under SAG (Bala et al., 2008; Govindasamy & Caldeira, 2000; Jones et al., 2018; Robock et al., 2008; Tjiputra et al., 2016; Xu et al., 2020). There is also the weakening of rainfall over the monsoon land regions such as the WASM region under SAG (e.g., Cheng et al., 2019; Dagon & Schrag, 2016, 2017; Haywood et al., 2013; Niemeier et al., 2013; Robock et al., 2008; Tilmes et al., 2013). In addition, it has been argued that use of stratospheric sulfate aerosol injection into the northern hemisphere only could induce drought in the Sahel, whereas stratospheric sulfate aerosol injection in only the Southern Hemisphere may lead to a significant increase in the Sahel vegetation productivity (Haywood et al., 2013). These authors found that SAG in only one hemisphere could impact the position of the Inter tropical Convergence Zone (ITCZ). Recently, studies indicate that the control of temperature gradient through multiple aerosol injection at several latitudes, as in the Geoengineering Large Ensembles (GLENS) simulations (Tilmes et al., 2018), leads to reduce shifts in the latitude of the ITCZ and related rainfall (Cheng et al., 2019; Kravitz et al., 2017, 2019; MacMartin et al., 2019; Tilmes et al., 2018; Xu et al., 2020).

To interpret changes in the global mean precipitation, Kravitz et al. (2013) characterized changes in the surface and atmospheric energy budgets using the Geoengineering Model Intercomparison Project (Kravitz & Robock, 2011) and they found that precipitation changes can be related to a reduction in mean evaporative moisture flux and increased moisture convergence, particularly over land regions. In addition, based on the same Geoengineering Model Intercomparison Project models (used by Kravitz et al., 2013), Tilmes et al. (2013) showed that although the large decrease in evaporation over land for most regions is consistent with the global precipitation reduction, this is not the case in the summer monsoon rainfall regions, such as the West Africa region, as summer monsoon rainfall is influenced by both local and large-scale processes. Therefore, the mechanisms responsible for changes in WASM precipitation remain to be clarified.

It has been demonstrated that changes to tropical precipitation can be usefully decomposed into the contributions from both thermodynamic and dynamic processes (e.g., Weller et al., 2019), and the decomposition methodology of Chadwick et al. (2013, 2016) can be used to quantify the relative contribution of these two terms (Chadwick et al., 2016; Kent et al., 2015; Lazenby & Todd, 2018; Monerie et al., 2019). Using this method, changes in tropical precipitation, under climate change, have been largely related to changes in the dynamical component which indicate shifts in the position of convection (e.g., Chadwick et al., 2016; Kent et al., 2015). Due to the great importance of WASM rainfall on agriculture productivity, hydroelectric power generation, and the water availability (e.g., Adarsh & Reddy, 2015), we decide to investigate changes in rainfall over the West Africa under SAG.

The objective of this paper is to use GLENS simulations (described in detail by Tilmes et al., 2018) to (1) improve our understanding on the potential impact of SAG on WASM precipitation and to (2) identify causes of WASM precipitation changes under SAG by applying the decomposition method of Chadwick et al. (2013, 2016) for precipitation changes with GLENS simulations.

The structure of the manuscript is as follows: The methods used in the study is explained in section 2, the main results are shown in section 3, and a discussion and conclusion are provided in section 4.

2. Methods

To assess the impact of SAG on WASM precipitation, we use simulations provided by GLENS project (Tilmes et al., 2018). The GLENS simulations are conducted with the Community Earth System Model version 1 (CESM1), which integrate the Whole Atmosphere Community Climate Model as the atmospheric component and fully coupled to ocean, land, and sea ice models (Mills et al., 2017). The horizontal resolution of the atmospheric component is 0.9° in latitude by 1.25° in longitude. These simulations are based on greenhouse gas (GHG) concentrations that follow the Representative Concentration Pathway 8.5 (RCP8.5; i.e., a high anthropogenic emission scenario). For the simulations of RCP8.5, a 20-member ensemble was carried out over the period 2010–2030, with three ensemble members expanded until 2097. The SAG simulations in which sulfur dioxide (SO_2) is injected into the stratosphere at four different latitudes simultaneously (15°N and 15°S at 25 km, 30°N and 30°S at 22.8 km, all at longitude of 180°; Kravitz et al., 2017; Tilmes et al., 2018) were derived from each of the 20 RCP8.5 simulations in 2020 and expanded until 2099. As in Pinto et al. (2020), the GLENS data set used in this study are composed of three members available at the moment of this analysis. The SO_2 injection is used to keep the global mean temperature, the interhemispheric temperature gradient, and the equator-to-pole temperature gradient at 2020 levels (Kravitz et al., 2017; Tilmes et al., 2018).

It has been demonstrated that the processes involved in the conversion of SO_2 into sulfate aerosols are well represented in the model (Mills et al., 2017). Also, it has been shown that the model correctly reproduces the observed aerosol optical depth after explosive volcanic eruptions, which gives us confidence for the model-simulated climate response to SAG (see Mills et al. (2016, 2017) for further details on the model description and validation procedure). A more detailed description about the data and simulations used in this study is available in Kravitz et al. (2017) and Tilmes et al. (2018).

To evaluate the capacity of the model to reproduce the WASM precipitation, we also use in this study, over 1990–2009, the precipitation from historical simulation (HIST) of GLENS (Tilmes et al., 2018) and two precipitation data sets which combine measurements from rain gauges and from satellite infrared and microwave sensors, the Global Precipitation Climatology Project (GPCP; Adler et al., 2003) and the Climate Prediction Center's Merged Analysis of Precipitation (CMAP; Xie & Arkin, 1997). The monthly mean monsoon precipitation simulated by the model is compared with those obtained with GPCP and CMAP data over the study region. The monsoon period is defined as the period from July to October (JASO). After the model evaluation, second, we examine changes in monsoon precipitation. To that end, we consider the ensemble mean monthly monsoon precipitation of RCP8.5 during 2010–2029 as the baseline (present-day climate). Then, for the climate changes under RCP8.5, we use the ensemble mean monthly monsoon precipitation of RCP8.5 simulations during 2050–2069 relative to the baseline and for the climate changes under SAG (our primary focus); we consider the ensemble mean monthly monsoon precipitation of the geoengineering simulations over 2050–2069, relative to the baseline. It has been shown that the relative distribution of SO_2 injection rates converges around 2050 (MacMartin et al., 2019). As the baseline period is 20 years (2010–2029), we also considered the 20 years following 2050 (i.e., 2050–2069) for geoengineering simulations. The statistical significance of precipitation changes obtained is determined using a two-sided t test, and the standard error is used to provide an error estimate of rainfall changes.

To investigate causes of changes in WASM precipitation, we use the framework developed in Chadwick et al. (2013, 2016). This method considers that precipitation, in the tropics, is dominated by convection (Chadwick et al., 2013, 2016). It shows that precipitation (P) at each grid point could be equivalent to a proxy for convective mass flux from the boundary layer to the free troposphere M* multiplied by the near surface specific humidity in the boundary layer q (Held & Soden, 2006; Kent et al., 2015; Lazenby & Todd,

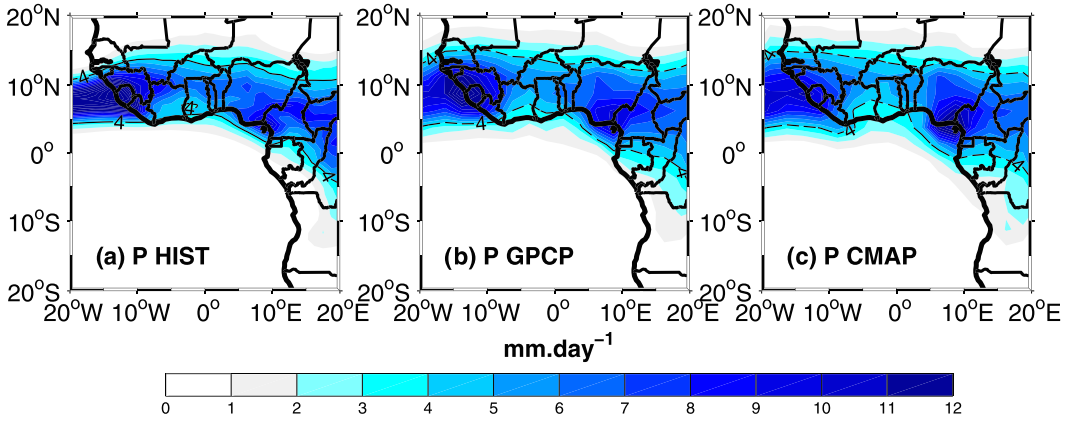

Figure 1. Spatial pattern of mean monthly JASO (July to October) precipitation computed for 1990–2009 in the West Africa from (a) model, (b) GPCP, and (c) CMAP. The units are mm. day $^{-1}$.

2018; Monerie et al., 2019): P = M*q. Therefore, changes in precipitation (ΔP) can be written as follows: $\Delta P = M^{*}\Delta q + q\Delta M^{*} + \Delta q\Delta M^{*} = \Delta P_{therm} + \Delta P_{dyn} + \Delta P_{cross}$.

where ΔP_{therm} is the thermodynamic change due to changes in specific humidity (q), ΔP_{dyn} represents the dynamic change term due to tropical circulation changes (M*), and ΔP_{cross} is the nonlinear cross term due to changes in both specific humidity and circulation. This method used here offers the possibility to separate changes in the dynamic term into the term associated with spatial shifts in the pattern of tropical circulation $\Delta P_{shift} = q\Delta M^{*}_{shift}$ and a term related to the tropical weakening circulation $\Delta P_{weak} = q\Delta M^{*}_{weak}$. Here $\Delta M^{*}_{weak} = -\alpha M^{*}$ and represents the tropical Atlantic-wide weakening circulation with $\alpha = -$ (tropical Atlantic mean ΔM*)/(tropical Atlantic mean M*) is defined to be constant throughout the tropical Atlantic (30°N–30°S, 60°W–20°E). The quantity ΔM^{*}_{shift} is deduced as the residual between ΔM* and ΔM^{*}_{weak} (i.e., $\Delta M^{*}_{shift} = \Delta M^{*} - \Delta M^{*}_{weak}$).

3. Results

3.1. Evaluation of Model Performance in Simulating WASM Precipitation

The spatial distribution of the mean rainfall in the boreal summer monsoon season (JASO) is presented in Figure 1. In general, model and the observation products show similar spatial precipitation patterns with maximum values within the vicinity of the Fouta Djallon highlands (5°–12 N, 5°–15°W), and the Cameroonian highlands and Jos Plateau in Nigeria at about 4°–10°N, 5°–14°E. However, although the localizations of these maxima are relatively well simulated, they differ in their intensity (Figure S1 in the supporting information). For example, the maximum precipitation over the Cameroonian highlands and Jos Plateau in Nigeria is underestimated by the model while precipitation simulated is overestimated in the region of Sierra Leone (6°–10°N, 10°–12°W). These model biases over the mountainous areas may be associated with the poor simulation of orographic forced ascent (e.g., Akinsanola et al., 2015; Akinsanola & Zhou, 2018) or the large uncertainty in the model precipitation estimates over this region (Akinsanola & Zhou, 2018; Diallo et al., 2016).

The monsoon system over West Africa is strongly related to the northward migration of the ITCZ during boreal spring and summer (Akinsanola & Zhou, 2018; Janicot et al., 2010; Sultan & Janicot, 2000). This migration is characterized by an abrupt latitudinal shift of the ITCZ from 5°N in June to 10°N in August, also known as the monsoon jump (Akinsanola et al., 2016; Akinsanola & Zhou, 2018; Berthou et al., 2019; Janicot et al., 2010; Sultan & Janicot, 2000). As such, behavior of the ITCZ is best characterized by a cross section of time latitude (Hovmöller diagram), the mean seasonal cycles of rainfall of the West African Monsoon, averaged between longitude 10°W and 10°E, are presented in Figure 2 through a Hovmöller diagram for the model and the two observation products (GPCP and CMAP). These figures indicate that while the observed monsoon jump is reproduced by the model, the model shows a greater intensity of precipitation than seen in observations (as already explained above). This monsoon jump is associated, both in model and

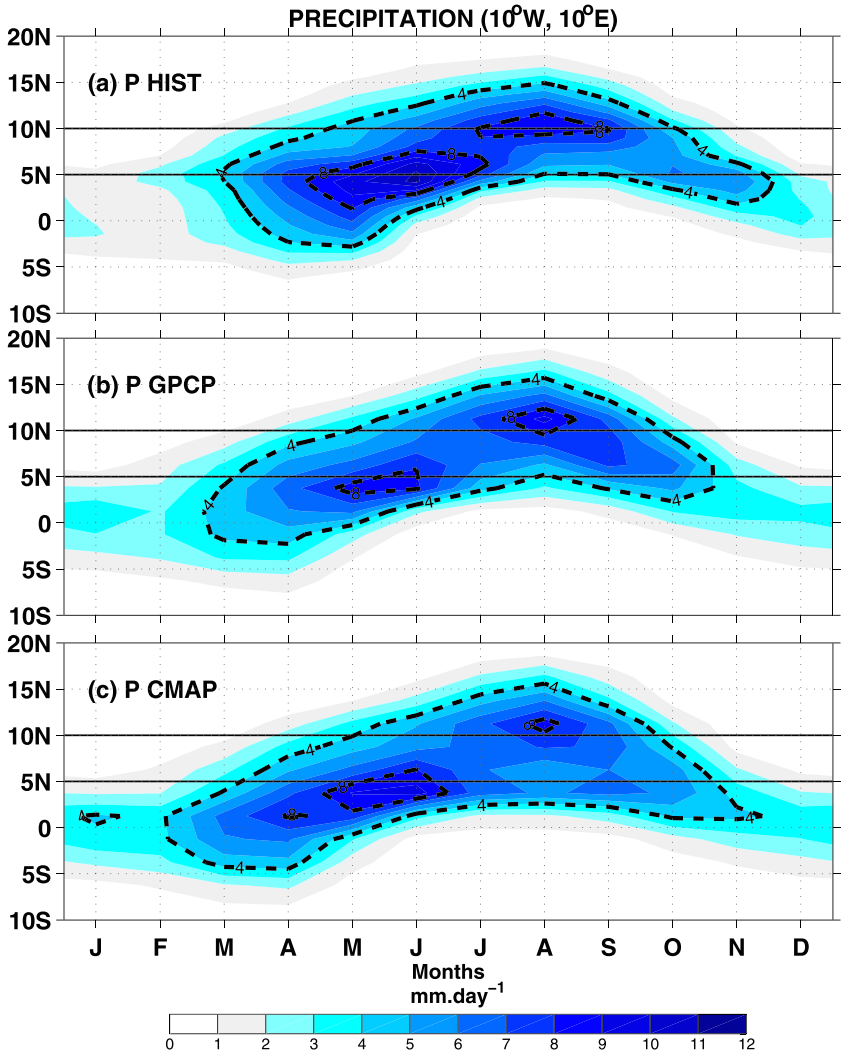

Figure 2. Hovmöller diagram of mean monthly rainfall averaged over longitude 10°W–10°E for the period 1990–2009 for (a) model, (b) GPCP, and (c) CMAP. In the Figures, the horizontal black line at 5°N is used to approximate the Guinean coast and the one at 10°N is used to indicate the arrival of monsoon rainfall in the Sahel region. The units are mm. day $^{-1}$.

observations, with strong precipitation in the Sahel region with maximum rainfall around 11°N in August while there is an abrupt cessation of rainfall intensities along the Guinean coast located at approximately 5°N (Figure 2). Then, from September to October, the monsoon rains weaken and gradually retreat to the south, toward the Guinea coast. Together these findings indicate the model is able to reproduce the basic climatological features of WASM precipitation.

3.2. Changes in the WASM Precipitation and Associated Causes

Figure 3 shows the response of monsoon season precipitation under RCP8.5 over the period 2050–2069 relative to baseline (RCP8.5 2010–2029) and decomposes this precipitation response into the various components as described in section 2. Relative to the baseline, the spatial patterns of the RCP8.5 simulations indicate a general increase in summer monsoon rainfall over West Africa with a significant increase in precipitation above 10°N in the Sahel regions (Figure 3a). However, below 10°N, toward the Guinean coast, changes in WASM precipitation are not significant. To understand the processes driving these WASM precipitation changes under RCP8.5, the precipitation changes (ΔP) are decomposed into their thermodynamic (ΔP_{therm}, driven by changes in specific humidity), dynamic (ΔP_{dyn}, driven by changes in the tropical

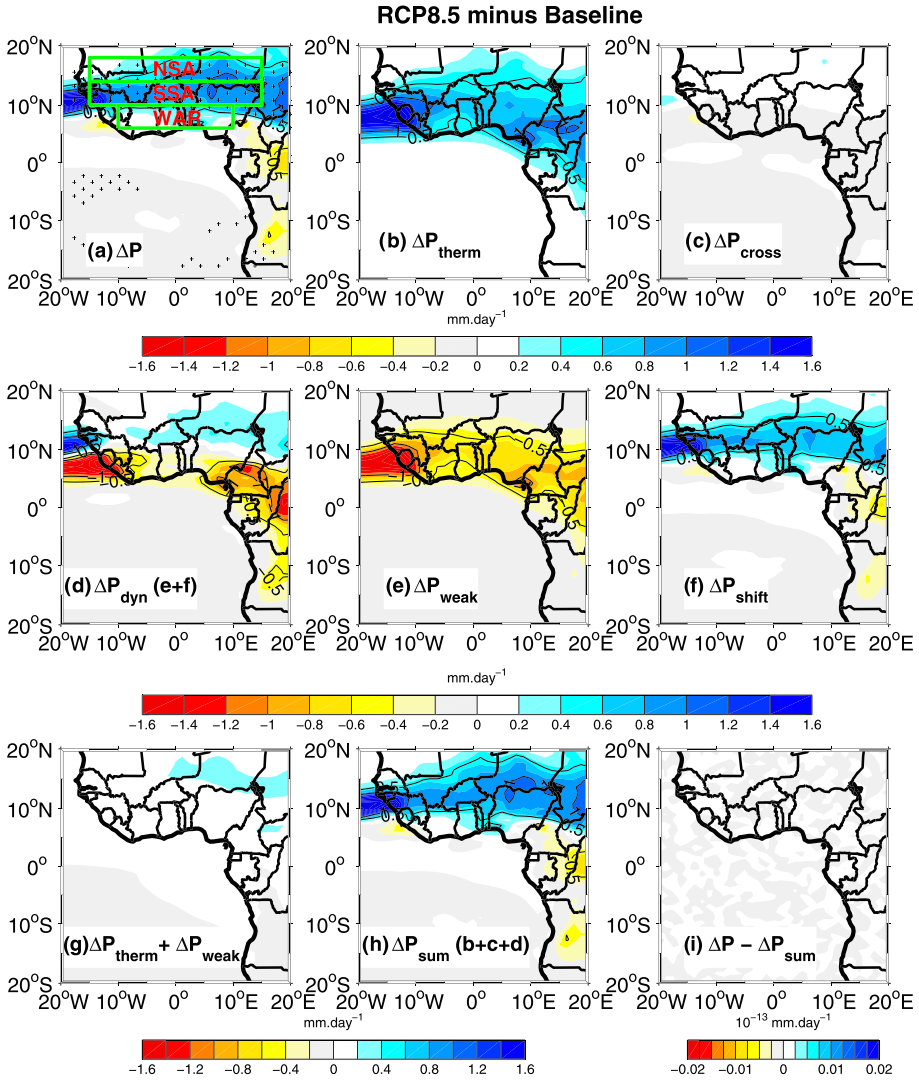

Figure 3. Decomposition of the (a) changes in WASM precipitation (ΔP) under RCP8.5 into its components, (b) thermodynamic (ΔP_{therm}), (c) nonlinear cross term (ΔP_{cross}), and (d) dynamic (ΔP_{dyn}). The dynamic component (ΔP_{dyn}) is divided into (e) a term associated with the weakened tropical circulation (ΔP_{weak}) and (f) a term associated with spatial shifts in the pattern of tropical circulation (ΔP_{shift}). Figure (g) shows the sum of $\Delta P_{therm} + \Delta P_{weak}$, (h) presents the sum of $\Delta P_{therm} + \Delta P_{cross} + \Delta P_{dyn}$ (components of precipitation change based on the decomposition method, i.e., terms b + c + d), and (i) the difference between (a) (the model precipitation change) and (h) (the sum of all the components of precipitation change). July to October (JASO) is used for the monsoon period. Changes in precipitation are obtained using the RCP8.5 ensemble mean over the period 2050–2069 minus the baseline RCP8.5 2010–2029 ensemble mean. The marked points in (a) indicate regions where changes in rainfall are statistically significant at the 95% level using the Student's *t* test. Boxes shown in (a) indicate the three specific regions used in this study. All units are mm. day $^{-1}$.

circulation), and nonlinear cross (ΔP_{cross}, driven by both changes in specific humidity and circulation) components (Figures 3b–3d). The contribution of ΔP_{cross} to rainfall changes is negligible (Figure 3c). ΔP_{therm} increases precipitation everywhere, though with the largest increases between 5°N and 15°N (Figure 3b). This contribution of ΔP_{therm} is due to the increase of near surface specific humidity relative to the baseline (Figures 4a and 4b), which contributes to intensify the climatological precipitation pattern (Figure 1). ΔP_{dyn} on the other hand leads to a large decrease in rainfall around 10°N up to the Guinean coast whereas it tends to slightly increase rainfall above 10°N. The dynamic term is strongly related to changes in the low-level monsoon winds relative to the baseline (Figures 4a and 4b) which results from changes in the sea-land thermal contrast (e.g., Li et al., 2019).

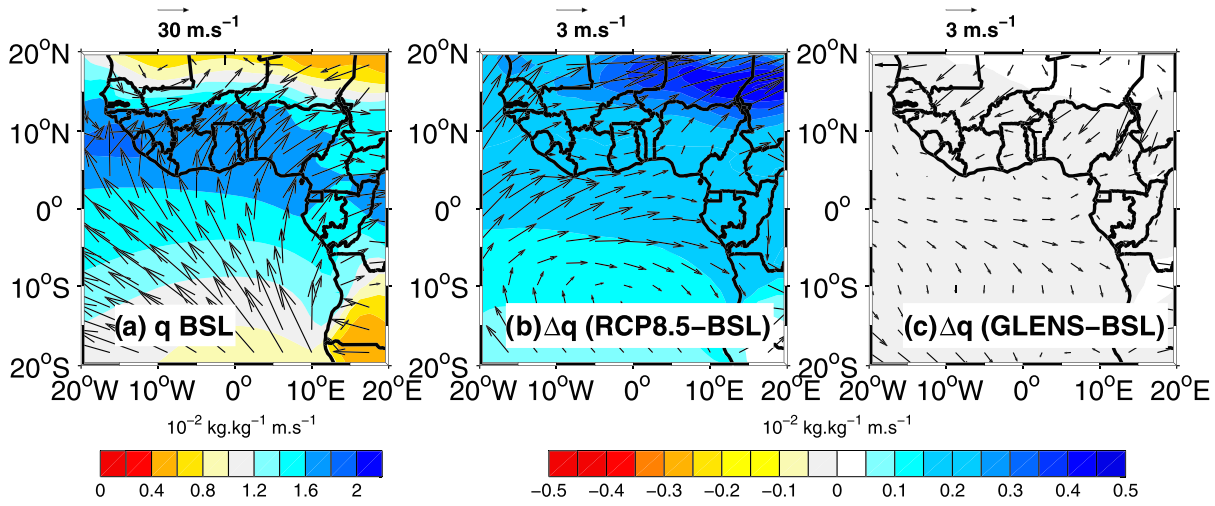

Figure 4. (a) Spatial pattern of JASO (July to October) surface specific humidity (color shading) and 957 hPa wind field (vectors) for the baseline RCP8.5 2010–2029 ensemble mean, (b) changes (relative to the baseline) in mean JASO surface specific humidity (color shading) and 957 hPa wind field (vectors) under RCP8.5 2050–2069 and (c) same as in (b) but under GLENS 2050–2069. The units are kg. kg $^{-1}$ m. s $^{-1}$ for specific humidity and m. s $^{-1}$ for the low-level wind field.

As under RCP8.5, the land would warm more rapidly than the ocean, the low-level land-sea thermal contrast would increase (Christensen et al., 2013) and this suggests that the position of ITCZ will be farther north than its climatological position. Using the simulations used in this study and following the method applied in Kravitz et al. (2016), Cheng et al. (2019) have shown that during the boreal summer there is a northward shift of the ITCZ by around 0.6° under RCP8.5. Thus, the precipitation band is located farther north compared to the climatological rain band and this explains why we have more precipitation (relative to the baseline) in the north of 10°N and less precipitation south of 10°N.

To better understand ΔP_{dyn} term, we follow Chadwick et al. (2013 and 2016) and split it into a term associated with the weakened low-level monsoon winds (ΔP_{weak}) and a term associated with the local dynamic response that shifts monsoon precipitation pattern (ΔP_{shift}). The spatial patterns of ΔP_{weak} is negative everywhere and acts to offset some of the increase in precipitation due to ΔP_{therm} (Figures 3b and 3e). However, the magnitude of ΔP_{therm} is slightly larger than that of ΔP_{weak}, and therefore, the sum of these two terms remains slightly positive in some areas in the northern Sahel (Figure 3g). Moreover, the spatial patterns of ΔP_{shift} are similar to that of ΔP (Figures 3a and 3f) and this term largely contributes to explain ΔP. Note that the change in WASM precipitation based on the decomposition method is equivalent to the change in precipitation from the model (Figures 3a and 3h) and the difference between these two terms is null (Figure 3i), showing that the decomposition method used is consistent to discuss changes in WASM rainfall. Thus, we conclude that, although the contribution of ΔP_{therm} to rainfall changes is not negligible, changes in WASM precipitation under RCP8.5 are mainly determined by the strong local dynamic response that shift monsoon precipitation northward by around 0.6 degree (relative to the baseline) due to increase in the land-sea thermal contrast in the lower troposphere.

Under GLENS, the spatial patterns of the SAG simulations relative to the baseline exhibit decrease in summer monsoon precipitation over the whole West Africa (Figure 5a). This rainfall decrease is not significant in the Sahel regions (north of 10°N) where precipitation increase was significant under global warming whereas south of 10°N below the Guinean coast (located around 5°N), the rainfall decrease is significant in the regions where the change in precipitation were not significant under the global warming (Figures 3a and 5a). As for RCP8.5, the contribution of ΔP_{cross} to rainfall changes is negligible for GLENS (Figure 5c). Contrary to RCP8.5, ΔP_{therm} makes a negligible contribution to rainfall changes under GLENS due to the small changes in the surface specific humidity relative to the baseline (Figures 4c and 5b). The sum of ΔP_{therm} and ΔP_{weak} is relatively small (Figure 5g), and thus, only the contribution of ΔP_{dyn} due to ΔP_{shift} is responsible for changes in rainfall (Figures 5d and 5f). The spatial patterns of ΔP_{shift} are similar to ΔP, and this term plays a major role in the precipitation changes. The contribution of ΔP_{shift} is largely associated with the low-level land-sea temperature contrast. As the solar radiation varies with the season and land

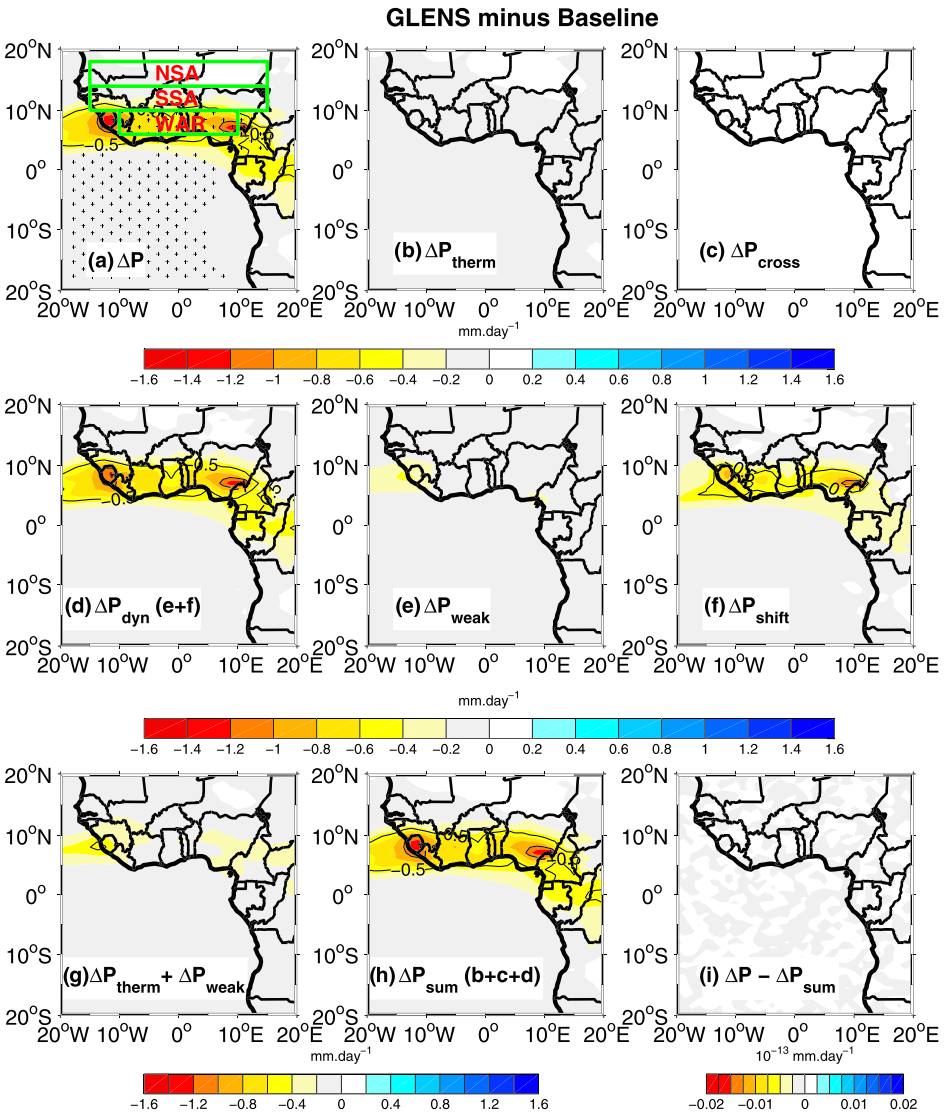

Figure 5. Same as in Figure 3 but for GLENS simulations.

would warm or cool faster than ocean (due to the heat capacity of water which is more important than that of the land), the low-level land-sea thermal contrast is strongly influenced by solar radiation (Liu et al., 2019). Therefore, the use of the SAG in the GLENS simulations to attenuate the amount of sunlight that reaches the Earth's surface will contribute to reduce the low-level land-sea thermal contrast. This reduction of land-sea thermal contrast leads to weak monsoon winds (Figures 4a and 4c) and a slight southward shift of the ITCZ (by around 0.18°) relative to the baseline (Cheng et al., 2019). The position of ITCZ is thus slightly shifted southward in GLENS relative to RCP8.5, but it remains further north relative to the climatological position of ITCZ. Thus, the decrease of rainfall noticed over the whole West Africa under GLENS is more pronounced in the south of 10°N. Here, also, the change in WASM precipitation under GLENS based on the decomposition method is equivalent to the change in precipitation from the model (Figures 5a and 5h) and the difference between these two terms is null (Figure 5i). In conclusion, under GLENS, changes in the WASM precipitation are largely driven by the reduced land-sea thermal contrast in the lower troposphere that leads to weakened monsoon circulation and a northward shift of the monsoon precipitation patterns.

In order to better quantify the impact of SAG on WASM precipitation, the West Africa domain considered in this work is divided into three specific areas indicated in Figures 3a and 5a: the Northern Sahel (NSA;

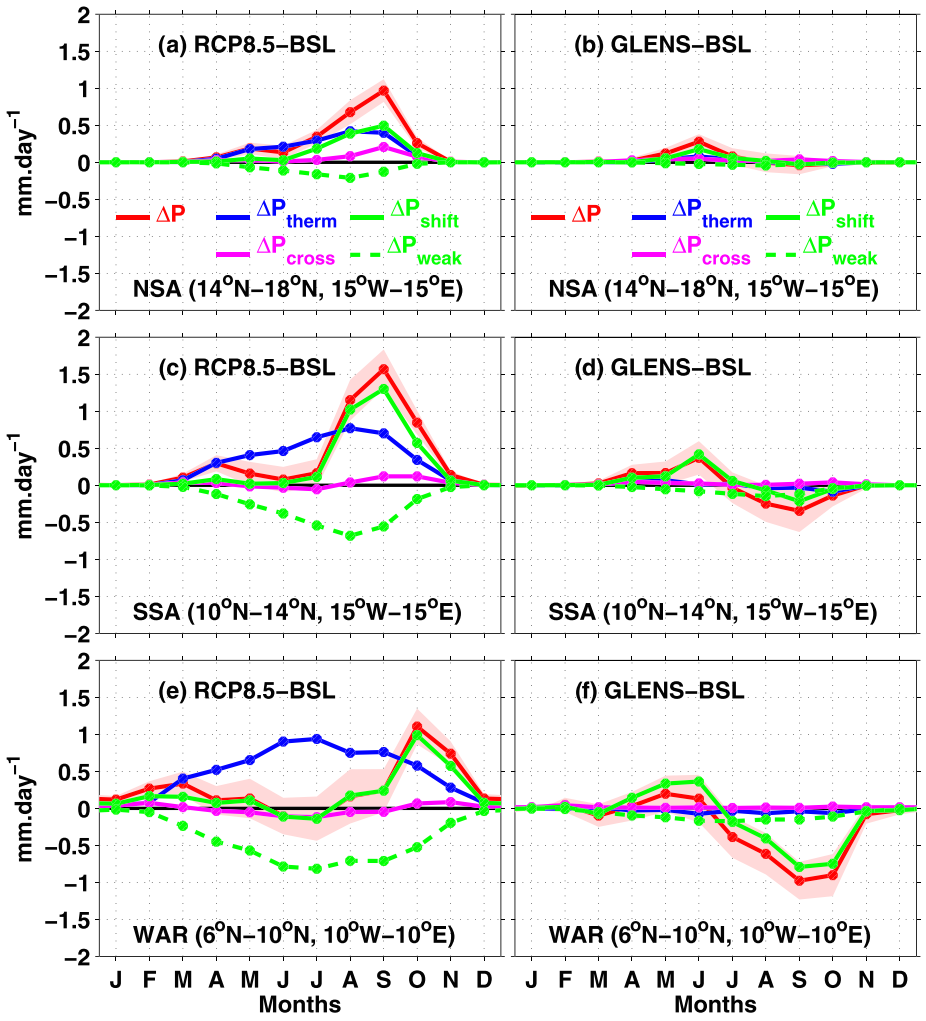

Figure 6. Seasonal cycles of precipitation changes and the different components of precipitation changes (see Figure 3) under RCP8.5 (left column) and GLENS (right column) relative to the baseline for the Northern of Sahel (a and b), Southern of Sahel (c and d), and the Western Africa region (e and f). Here the nonlinear component of precipitation (ΔP_{cross}) is added and the shaded areas indicating the standard error on the term of precipitation changes. Changes in precipitation are obtained as in Figures 3 and 5. All units are mm. day $^{-1}$.

18°N–14°N, 15°W–15°E), the Southern Sahel (SSA; 14°N–10°N, 15°W–15°E), and the Western Africa region (WAR; 6°N–10°N, 10°W–10°E). These regions are similar to those used in previous studies (e.g., Diaconescu et al., 2014; Soares et al., 2019). Figure 6 presents the seasonal cycles of precipitation changes for RCP8.5 and GLENS with its various components for the three different regions (NSA, SSA, and WAR). Under RCP8.5, large increase in rainfall appears only from July to October (which corresponds to the monsoon period considered in this study) and there is an increase of 0.56 ± 0.12 (44.76%), 0.93 ± 0.22 (19.74%), and 0.34 ± 0.30 mm (5.14%) compared with baseline in the Northern Sahel (NSA), Southern Sahel (SSA), and Western Africa region (WAR), respectively. However, under SRM, from July to October, the precipitation is nearly unchanged (0.00 ± 0.10 mm, i.e., 0.21%) in the NSA region but it decreases by 0.19 ± 0.22 mm (4.06%) and 0.72 ± 0.27 mm (10.87%) in SSA and WAR, respectively. In these three regions, during the boreal summer, changes in rainfall relative to the baseline for RCP8.5 and GLENS dominate changes in evaporation (Figure 7). Outside the monsoon season, under RCP8.5, although there is a general increase in precipitation and evaporation during the rest of the year, changes in evaporation dominate changes in precipitation (Figures 7a, 7c, and 7e). In GLENS, we note also an increase in precipitation during the nonmonsoon season, particularly in the boreal spring in all the three regions (Figures 7b, 7d, and 7f). However, the changes in rainfall are larger than those of evaporation in SSA and WAR regions while the change in rainfall is

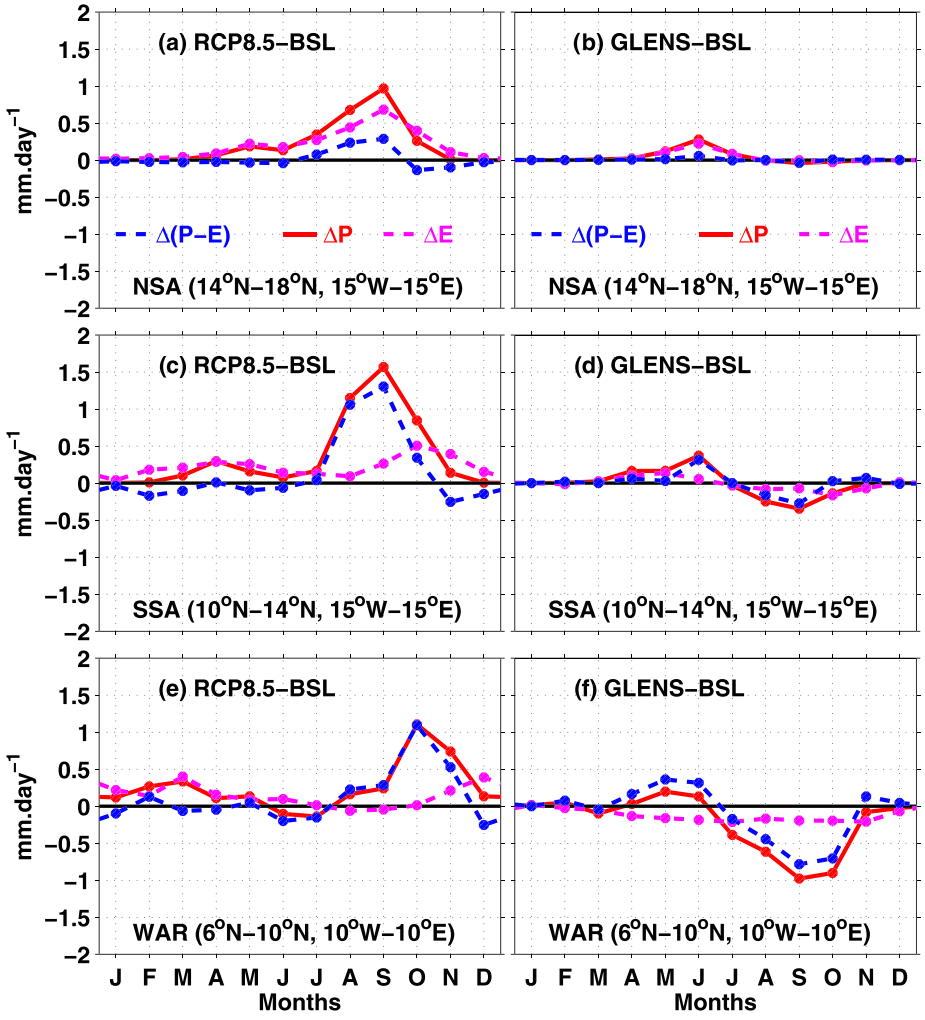

Figure 7. Seasonal cycles of precipitation, evaporation, and precipitation-evaporation changes (relative to the baseline) under RCP8.5 (left column) and GLENS (right column) for the Northern of Sahel (a and b), Southern of Sahel (c and d), and the Western Africa region (e and f). Changes are for the period 2050–2069 relative to the baseline. All units are mm. day $^{-1}$.

similar to that of evaporation in NSA region. Regarding the physical processes responsible for rainfall changes, Figure 6 also reveals that in the three regions, changes in precipitation under RCP8.5 are associated with the changes in the monsoon circulation that shifts monsoon precipitation northward due to increase in the low-level land-sea thermal contrast. However, it should be mentioned that in the NSA region, changes in thermodynamic component caused by increase in atmospheric specific humidity and the changes in the nonlinear cross term related to both changes in specific humidity and circulation also play nonnegligible role. Under GLENS, in the three regions, changes in rainfall are mainly determined by the reduction of the land-sea thermal contrast in the lower troposphere which leads to weakened monsoon circulation and a northward shift of the monsoon precipitation. All these results obtained here are consistent with those presented above for the three regions except for the NSA region where the contributions of the thermodynamic and nonlinear terms to rainfall changes are not negligible.

Following Cheng et al. (2019), the boreal summer (JASO) mean efficacy of geoengineering to counterbalance the effects of high GHGs emissions (ratio of Geoengineering–High-GHGs and High-GHGs–Baseline) is calculated for precipitation. The efficacy value >-1 indicates under compensation induced by geoengineering relative to baseline whereas the efficacy value <-1 suggests geoengineering-induced over compensation relative to baseline. We find that the mean efficacy value of precipitation is $-0.99 \approx -1$ (compensation),

−1.2 (slight over compensation), and −3.11 (high over compensation) for the NSA, SSA, and WAR regions, respectively. So, the use of SAG is effective for rainfall (i.e., SAG compensates changes in rainfall under RCP8.5) in the northern and southern Sahel and over-effective (i.e., SAG over compensates changes in precipitation under RCP8.5) in the Western Africa region. This suggests that offsetting all warming would be going too far if the goal were to restore the Western Africa monsoon precipitation; instead, this would require limiting SAG deployment to offsetting 1/3 of RCP8.5 warming. As the link between global mean warming and regional precipitation change is subject to large uncertainties, this model results should be considered with caution.

4. Conclusion and Discussion

Using results from the GLENS project which use the CESM1 (Whole Atmosphere Community Climate Model) model and stratospheric sulfate aerosols injection (at four different locations) to maintain global mean surface temperature and also the interhemispheric and equator-to-pole temperature gradients at their 2020 values under RCP8.5 scenario, we investigated the potential impact of SAG on WASM precipitation (defined over the period from July to October) and the drivers of this response. We found that simulated rainfall in GLENS reasonably reproduces the observed spatial patterns of WASM precipitation, including its characteristic northward jump over the season.

We focused our study on three specific regions which are the NSA, the SSA, and the WAR. Results showed that, under RCP8.5, during the monsoon period, precipitation increased by 44.76% (0.56 ± 0.12 mm), 19.74% (0.93 ± 0.22 mm), and 5.14% (0.34 ± 0.30 mm) compared with baseline in the NSA, SSA, and WAR regions, respectively. However, in GLENS, relative to the baseline, the WASM rainfall is practically unchanged (0.00 ± 0.10 mm) in the NSA region, but in SSA and WAR regions, rainfall is reduced by 4.06% (0.19 ± 0.22 mm) and 10.87% (0.72 ± 0.27 mm) during the monsoon period, respectively. Note that under GLENS, the change in rainfall is only significant in the WAR. Also, in this region, the mean efficacy ratio of SAG (−3.11) in rainfall calculated during the monsoon period suggests a high over compensation contrary to the NSA and SSA where there is a compensation (efficacy ratio is $-0.99 \approx -1$) and a slight over compensation (efficacy ratio is −1.2), respectively. Thus, the use of SAG is effective in the Sahel regions (NSA and SSA) whereas it is overeffective in the WAR. In this latter region, if the objective were to restore the Western African monsoon precipitation, this work suggests that the deployment of SAG should be limited to offset 1/3 of RCP8.5 warming.

In this study, we identified the physical mechanisms behind changes in WASM precipitation under RCP8.5 and GLENS, by applying the decomposition method developed in Chadwick et al. (2013, 2016). Results reveal that changes (increase) in WASM precipitation relative to the baseline under RCP8.5 are mainly caused by changes in the local dynamic response due to increase in the low-level land-sea thermal contrast that shift monsoon precipitation northward, whereas under GLENS, changes (decrease) in rainfall relative to the baseline are mainly determined by the reduction of the land-sea thermal contrast in the lower troposphere that leads to weakened monsoon circulation and a northward shift of the monsoon precipitation. We noted that under RCP85, the thermodynamic component related to the increase in specific humidity is practically compensated by the tropics-wide weakening tropical circulation and the response of these two terms seen under RCP8.5 are fully offset by SAG in GLENS.

In agreement with previous studies (e.g., Cheng et al., 2019), our results showed that WASM precipitation decrease under GLENS. This study provides light on the physical mechanisms responsible for rainfall changes in the WAR under GLENS. Our findings indicated that changes in rainfall in this region are largely driven by the changes in the monsoon circulation which result from the reduction of the thermal gradient induced by the use of SAG. Understanding the causes of the precipitation decrease will contribute to improve/initiate new strategies for stratospheric aerosol injection to attenuate rainfall changes in this region under SAG. Changes in mean precipitation are expected to have an impact on water availability, which is essential in this region, and has to be investigated in more detail. Here the decomposition method used to quantify physical processes driving changes in precipitation allowed to reconstruct the change in precipitation given by the model itself. Thus, this method could be usefully applied elsewhere in the tropics to assess rainfall changes under SAG. In this study, we have investigated monthly mean precipitation and evaporation changes. More work has to be done in order to identify impacts of changes in these changes on society for example on food production and water availability, which needs to be clarified in future studies.

Acknowledgments

We acknowledge the financial support of the DECIMALS fund of the Solar Radiation Management Governance Initiative, which was set up in 2010 by the Royal Society, Environmental Defense Fund and The World Academy of Sciences and is funded by the Open Philanthropy Project. The data used in this study are available to the community via the Earth System Grid (see information at www.cesm.ucar.edu/projects/community-projects/GLENS/). The CESM project is supported primarily by the National Science Foundation. This work is also in the framework of the Jeune Equipe Associée à l'IRD named Variabilité de la SAlinité et Flux d'eau doUce à Multi-Échelles which is supported by Institut de Recherche pour le Développement (IRD).

References

Adarsh, S., & Reddy, M. J. (2015). Trend analysis of rainfall in four meteorological subdivisions of southern India using non parametric methods and discrete wavelet transforms. *International Journal of Climatology*, *35*(1107–112), 4. https://doi.org/10.1002/joc.4042

Adler, R. F., Huffman, G. J., Chang, A., Ferraro, R., Xie, P.-P., Janowiak, J., et al. (2003). The version 2 Global Precipitation Climatology Project (GPCP) monthly precipitation analysis (1979–present). *Journal of Hydrometeorology*, *4*, 1147–1167. https://doi.org/10.1175/1525-7541(2003)004<1147:tvgpcp>2.0.co;2

Akinsanola, A. A., Ogunjobi, K. O., Ajayi, V. O., Adefisan, E. A., Omotosho, J. A., & Sanogo, S. (2016). Comparison of five gridded precipitation products at climatological scales over West Africa. *Meteorology and Atmospheric Physics*, *129*, 669–689. https://doi.org/10.1007/s00703-016-0493-6

Akinsanola, A. A., Ogunjobi, K. O., Gbode, I. E., & Ajayi, V. O. (2015). Assessing the capabilities of three regional climate models over CORDEX Africa in simulating West African summer monsoon precipitation. *Advances in Meteorology*, *2015*. https://doi.org/10.1155/2015/935431

Akinsanola, A. A., & Zhou, W. (2018). Ensemble-based CMIP5 simulations of West African summer monsoon rainfall: Current climate and future changes. *Theoretical and Applied Climatology*, *136*, 1021–1031. https://doi.org/10.1007/s00704-018-2516-3

Bala, G., Duffy, P. B., & Taylor, K. E. (2008). Impact of geoengineering schemes on the global hydrological cycle. *Proceedings of the National Academy of Sciences*, *105*(22), 7664–7669. https://doi.org/10.1073/pnas.0711648105

Berthou, S., Rowell, D. P., Kendon, E. J., Roberts, M. J., Stratton, R. A., Crook, J. A., & Wilcox, C. (2019). Improved climatological precipitation characteristics over West Africa at convection-permitting scales. *Climate Dynamics*, *53*, 1991–2011. https://doi.org/10.1007/s00382-019-04759-4

Chadwick, R., Boutle, I., & Martin, G. (2013). Spatial patterns of precipitation change in CMIP5: Why the rich do not get richer in the tropics. *Journal of Climate*, *26*(3), 803–3822. https://doi.org/10.1175/JCLI-D-12-00543.1

Chadwick, R., Good, P., & Willett, K. (2016). A simple moisture advection model of specific humidity change over land in response to SST warming. *Journal of Climate*, *29*(21), 7613–7632. https://doi.org/10.1175/JCLI-D-16-0241.1

Cheng, W., MacMartin, D. G., Dagon, K., Kravitz, B., Tilmes, S., Richter, J. H., et al. (2019). Soil moisture and other hydrological changes in a stratospheric aerosol geoengineering large ensemble. *Journal of Geophysical Research: Atmospheres*, *124*, 12,773–12,793. https://doi.org/10.1029/2018JD030237

Christensen, J. H., Krishna Kumar, K., Aldrian, E., An, S.-I., Cavalcanti, I. F. A., de Castro, M., et al. (2013). Climate phenomena and their relevance for future regional climate change. In T. F. Stocker (Ed.), *Climate Change 2013: The physical Science Basis. Contribution of Working Group I to the Fifth Assessment Report of the Intergovernmental Panel on Climate Change*, (1217–1308). Cambridge, UK and New York: Cambridge University Press.

Crutzen, P. J. (2006). Albedo enhancement by stratospheric sulfur injections: A contribution to resolve a policy dilemma? *Climatic Change*, *77*(3–4), 211–220. https://doi.org/10.1007/s10584-006-9101-y

Dagon, K., & Schrag, D. P. (2016). Exploring the effects of solar radiation management on water cycling in a coupled land–atmosphere model. *Journal of Climate*, *29*(7), 2635–2650. https://doi.org/10.1175/JCLI-D-15-0472.1

Dagon, K., & Schrag, D. P. (2017). Regional climate variability under model simulations of solar geoengineering. *Journal of Geophysical Research: Atmospheres*, *122*, 12,106–12,121. https://doi.org/10.1002/2017JD027110

Diaconescu, E. P., Gachon, P., Scinocca, J. and Laprise, R. (2014). Evaluation of daily precipitation statistics and monsoon onset/retreat over western Sahel in multiple data sets. *Climate Dynamics*, 1–31. https://doi.org/10.1007/s00382-014-2383-2

Diallo, I., Giorgi, F., Tall, M., Mariotti, L., & Gaye, A. T. (2016). Projected changes of summer monsoon extreme and hydroclimatic regimes over West Africa for the twenty-first century. *Climate Dynamics*, *47*, 3931–3954. https://doi.org/10.1007/s00382-016-3,052-4

Giannini, A., Lyon, B., Seager, R., & Vigaud, N. (2018). Dynamical and thermodynamic elements of modeled climate change at the East African margin of convection. *Geophysical Research Letters*, *45*, 992–1000. https://doi.org/10.1002/2017GL075486

Govindasamy, B., & Caldeira, K. (2000). Geoengineering Earth's radiation balance to mitigate CO2 -induced climate change. *Geophysical Research Letters*, *27*, 2141–2144. https://doi.org/10.1029/1999GL006086

Haywood, J. M., Jones, A., Bellouin, N., & Stephenson, D. (2013). Asymmetric forcing from stratospheric aerosols impacts Sahelian rainfall. *Nature Climate Change*, *3*(7), 660–665. https://doi.org/10.1038/nclimate1857

Held, I. M., & Soden, B. J. (2006). Robust responses of the hydrological cycle to global warming. *Journal of Climate*, *19*(21), 5686–5699. https://doi.org/10.1175/JCLI3990.1

Irvine, P., Emanuel, K., He, J., Horowitz, L. W., Vecchi, G., & Keith, D. (2019). Halving warming with idealized solar geoengineering moderates key climate hazards. *Nature Climate Change*, *9*(4), 295–299. https://doi.org/10.1038/s41558-019-0398-8

Janicot, S., Mounier, F., Gervois, S., Sultan, B., & Kiladis, G. (2010). The dynamics of the West African monsoon Part V: The role of convectively coupled equatorial Rossby waves. *Journal of Climate*, *23*. https://doi.org/10.1175/2010JCLI3221.1

Jiang, J., Cao, L., MacMartin, D. G., Simpson, I. R., Kravitz, B., Cheng, W., et al. (2019). Stratospheric sulfate aerosol geoengineering could alter the high-latitude seasonal cycle. *Geophysical Research Letters*, *46*, 14,153–14,163. https://doi.org/10.1029/2019GL085758

Jones, A. C., Hawcroft, M. K., Haywood, J. M., Jones, A., Guo, X., & Moore, J. C. (2018). Regional climate impacts of stabilizing global warming at 1.5 k using solar geoengineering. *Earth's Future*, *6*, 230–251. https://doi.org/10.1002/2017EF000720

Keith, D. W. (2000). Geoengineering the climate: History and prospect. *Annual Review of Energy and the Environment*, *25*(1), 245–284. https://doi.org/10.1146/annurev.energy.25.1.245

Kent, C., Chadwick, R., & Rowell, D. P. (2015). Understanding uncertainties in future projections of seasonal tropical precipitation. *Journal of Climate*, *28*(4), 390–4413. https://doi.org/10.1175/JCLI-D-14-00613.1

Kravitz, B., Caldeira, K., Boucher, O., Robock, A., Rasch, P. J., Alterskjær, K., et al. (2013). Climate model response from the Geoengineering Model Intercomparison Project (GeoMIP). *Journal of Geophysical Research: Atmospheres*, *118*, 8320–8332. https://doi.org/10.1002/jgrd.50646

Kravitz, B., MacMartin, D. G., Mills, M. J., Richter, J. H., Tilmes, S., Lamarque, J. F., et al. (2017). First simulations of designing stratospheric sulfate aerosol geoengineering to meet multiple simultaneous climate objectives. *Journal of Geophysical Research: Atmospheres*, *122*, 12,616–12,634. https://doi.org/10.1002/2017JD026874

Kravitz, B., MacMartin, D. G., Tilmes, S., Richter, J. H., Mills, M. J., Cheng, W., et al. (2019). Comparing surface and stratospheric impacts of geoengineering with different SO_2 injection strategies. *Journal of Geophysical Research: Atmospheres*, *124*, 7900–7918. https://doi.org/10.1029/2019JD030329

Kravitz, B., MacMartin, D. G., Wang, H., & Rasch, P. J. (2016). Geoengineering as a design problem. *Earth System Dynamics*, *7*, 469–497. https://doi.org/10.5194/esd-7-469-2016

Kravitz, B., & Robock, A. (2011). Climate effects of high-latitude volcanic eruptions: Role of the time of year. *Journal of Geophysical Research*, *116*, D01105. https://doi.org/10.1029/2010JD014448

Lazenby, & Todd (2018). Future precipitation projections over central and southern Africa and the adjacent Indian Ocean: What causes the changes and the uncertainty? *Journal of Climate*, *31*, 4807–4826. https://doi.org/10.1175/JCLI-D-17-0311.1

Li, Z., Sun, Y., Li, T., Ding, Y., & Hu, T. (2019). Future changes in East Asian summer monsoon circulation and precipitation under 1.5 to 5 °C of warming. *Earth's Future*, *7*, 1391–1406. https://doi.org/10.1029/2019EF001276

Liu, Y., Cai, W., Sun, C., Song, H., Cobb, K. M., Li, J., et al. (2019). Anthropogenic aerosols cause recent pronounced weakening of Asian Summer Monsoon relative to last four centuries. *Geophysical Research Letters*, *46*, 5469–5479. https://doi.org/10.1029/2019GL082497

MacMartin, D. G., Ricke, K. L., & Keith, D. W. (2018). Solar geoengineering as part of an overall strategy for meeting the 1.5 °C Paris target. *Philosophical Transactions of the Royal Society A*, *376*, 20160454. https://doi.org/10.1098/rsta.2016.0454

MacMartin, D. G., Wang, W., Kravitz, B., Tilmes, S., Richter, J. H., & Mills, M. J. (2019). Timescale for detecting the climate response to stratospheric aerosol geoengineering. *Journal of Geophysical Research: Atmospheres*, *124*, 1233–1247. https://doi.org/10.1029/2018JD028906

Mills, M. J., Richter, J. H., Tilmes, S., Kravitz, B., MacMartin, D. G., Glanville, A. A., et al. (2017). Radiative and chemical response to interactive stratospheric sulfate aerosols in fully coupled CESM1(WACCM). *Journal of Geophysical Research: Atmospheres*, *122*, 13,061–13,078. https://doi.org/10.1002/2017JD027006

Mills, M. J., Schmidt, A., Easter, R., Solomon, S., Kinnison, D. E., Ghan, S. J., et al. (2016). Global volcanic aerosol properties derived from emissions, 1990–2014, using CESM1(WACCM). *Journal of Geophysical Research: Atmospheres*, *121*, 2332–2348. https://doi.org/10.1175/JCLI-D-12-00558.1

Monerie, P. A., Fontaine, B., & Roucou, P. (2012). Expected future changes in the African monsoon between 2030 and 2070 using some CMIP3 and CMIP5 models under a medium-low RCP scenario. *Journal of Geophysical Research*, *117*, D16111. https://doi.org/10.1029/2012JD017510

Monerie, P.-A., Robson, J., Dong, B., Hodson, D. L. R., & Klingaman, N. P. (2019). Effect of the Atlantic multidecadal variability on the global monsoon. *Geophysical Research Letters*, *46*, 1765–1775. https://doi.org/10.1029/2018GL080903

Niemeier, U., Schmidt, H., Alterskjær, K., & Kristjánsson, J. E. (2013). Solar irradiance reduction via climate engineering: Impact of different techniques on the energy balance and the hydrological cycle. *Journal of Geophysical Research: Atmospheres*, *118*, 11,905–11,917. https://doi.org/10.1002/2013JD020445

Odoulami, R. C., & Akinsanola, A. A. (2017). Recent assessment of West African summer monsoon daily rainfall trends. *Weather*, *73*. https://doi.org/10.1002/wea.2965

Pinto, I., Jack, C., Lennard, C., Tilmes, S., & Odoulami, R. C. (2020). Africa's climate response to solar radiation management with stratospheric aerosol. *Geophysical Research Letters*, *47*, e2019GL086047. https://doi.org/10.1029/2019GL086047

Robock, A., Oman, L., & Stenchikov, G. L. (2008). Regional climate responses to geoengineering with tropical and Arctic SO_2 injections. *Journal of Geophysical Research*, *113*, D16101. https://doi.org/10.1029/2008JD010050

Soares, P. M. M., Careto, J. A. M., Cardoso, R. M., Goergen, K., & Trigo, R. M. (2019). Land-atmosphere coupling regimes in a future climate in Africa: From model evaluation to projections based on. *CORDEX-Africa. Journal of Geophysical Research: Atmospheres*, *124*. https://doi.org/10.1029/2018JD029473

Sultan, B., & Janicot, S. (2000). Abrupt shift of the ICTZ over West Africa and intra-seasonal variability. *Geophysical Research Letters*, *27*, 3353–3356. https://doi.org/10.1029/1999GL011285

Tilmes, S., Fasullo, J., Lamarque, J. F., Marsh, D. R., Mills, M., Alterskjær, K., et al. (2013). The hydrological impact of geoengineering in the Geoengineering Model Intercomparison Project (GeoMIP). *Journal of Geophysical Research: Atmospheres*, *118*, 11,036–11,058. https://doi.org/10.1002/jgrd.50868

Tilmes, S., Richter, J. H., Kravitz, B., MacMartin, D. G., Mills, M. J., Simpson, I. R., et al. (2018). CESM1(WACCM) Stratospheric Aerosol Geoengineering Large Ensemble (GLENS) Project. *Bulletin of the American Meteorological Society*, *99*. https://doi.org/10.1175/BAMS-D-17-0267.1

Tjiputra, J. F., Grini, A., & Lee, H. (2016). Impact of idealized future stratospheric aerosol injection on the large-scale ocean and land carbon cycles. *Journal of Geophysical Research: Biogeosciences*, *121*, 2–27. https://doi.org/10.1002/2015JG003045

Weller, E., Jakob, C., & Reeder, M. J. (2019). Understanding the dynamic contribution to future changes in tropical precipitation from low-level convergence lines. *Geophysical Research Letters*, *46*, 2196–2203. https://doi.org/10.1029/2018GL080813

Xie, P. P., & Arkin, P. A. (1997). Global precipitation: A 17-year monthly analysis based on gauge observations, satellite estimates, and numerical model outputs. *Bulletin of the American Meteorological Society*, *78*, 2539–2558. https://doi.org/10.1175/1520-0477(1997)078<2539:gpayma>2.0.co;2

Xu, Y., Lin, L., Tilmes, S., Dagon, K., Xia, L., Diao, C., et al. (2020). Climate engineering to mitigate the projected 21st-century terrestrial drying of the Americas: Carbon Capture vs. Sulfur Injection? *Earth System Dynamics*. https://doi.org/10.5194/esd-2020-2